



ORIGINAL RESEARCH ARTICLE

Fatigue Performance of Low Pressure Carbonitrided 20MnCr5 and SAE 8620 Steel Alloys

Larissa Vilela Costa, Kip O. Findley, and Robert L. Cryderman

Submitted: 31 July 2023 / Accepted: 17 September 2023 / Published online: 12 October 2023

Low pressure carbonitriding and pressurized gas quenching heat treatments were conducted on four steel alloys. Bending fatigue tests were performed, and the highest endurance limit was attained by 20MnCr5 + B, followed by 20MnCr5, SAE 8620 + Nb, and SAE 8620. The differences in fatigue endurance limit occurred, despite similar case depths and surface hardness between alloys. Low magnitude tensile residual stresses were measured near the surface in all conditions. Additionally, non-martensitic transformation products (NMTPs) were observed to various extents near the surface. However, there were no differences in retained austenite profiles, and retained austenite was mostly stable against deformation-induced transformation to martensite during fatigue testing, contrasting some studies on carburized steels. The results suggest that the observed difference in fatigue lives is due to differences in chemical composition and prior austenite grain size. Alloys containing B and Nb had refined prior austenite grain sizes compared to their counterparts in each alloy class.

Keywords boron, fatigue, heat treatment, steel

1. Introduction

The automotive industry is constantly looking for ways to reduce the weight of mechanical components, such as gears, mainly due to economic and environmental reasons. Gears are a critical part of powertrain components in promoting high efficiency and durability. It is important to adequately select the steel alloy, manufacturing processes, and heat treatments, since they are critical for gear performance and structural integrity (Ref 1, 2). Gears are subject to cyclic loading during their operation, and consequently, fatigue performance is critical in their design as well.

Carbonitriding, which promotes diffusion of both carbon and nitrogen into steel components, has some advantages over carburizing such as higher hardness at the surface of the case and higher hardenability, allowing for less severe quenching (Ref 3-5). A gradient of carbon and nitrogen is formed from the

surface to the base composition in the core, causing a variation in the microstructure and hardness throughout the depth. The higher carbon and nitrogen content on the surface of the steel also increases solid solution strengthening. The microstructure and composition gradient also typically result in a compressive residual stress on the surface.

During carbonitriding, the volume of ammonia gas, time of treatment, temperature, furnace atmosphere, and furnace conditions affect the hardened case and contribute to mitigating the formation of undesirable transformation products in the case (Ref 3). One important consideration is nitrogen absorption into the steel, particularly in high temperature vacuum carbonitriding. Ammonia dissociation forms atomic nitrogen and hydrogen, which subsequently facilitates the diffusion of nitrogen into the steel. A competing process is the formation of molecular nitrogen (N₂), which suppresses the absorption of nitrogen into the steel.

When low pressure carbonitriding is performed, only the gases used for the treatment (hydrocarbon gases such as propane or acetylene and ammonia) are present in the furnace atmosphere, and the pressure used for the treatment is in the range of 5 to 20 mbar. These conditions are different from atmospheric carbonitriding, where hydrocarbon gases are typically mixed with air at a specific rate, forming an endogas composed of carbon monoxide (CO), hydrogen (H₂), nitrogen (N₂), and carbon dioxide (CO₂). If a combination of hydrocarbon gas and air is used, some water vapor is also part of the composition of endogas. Therefore, in gas carbonitriding or carburizing, carbon dioxide and water vapor are potential oxidizing agents present in the furnace atmosphere. Internal oxidation does not occur when the material is subjected to low pressure carbonitriding due to the considerable reduction of oxidizing gases in the furnace, which is a potential benefit for fatigue performance (Ref 6, 7).

A commonly used alloy in carbonitriding applications is the boron containing alloy 20MnCr5 + B. However, the role of boron in microstructure evolution and properties after carboni-

This article is an invited submission to the Journal of Materials Engineering and Performance selected from presentations at the 29th Heat Treating Society Conference and Exposition (Heat Treat 2017) held October 24–26, 2017, in Columbus, Ohio, and the 31st Heat Treating Society Conference and Exposition (Heat Treat 2021) held September 14–16, 2021, in St. Louis, Missouri. It has been expanded from the original presentation. The issue was organized by Robert Cryderman, Colorado School of Mines; Rob C. Goldstein, Fluxtrol; Collin A. Russell, Los Alamos National Laboratory; and John Tartaglia, Element Materials Technology.

Larissa Vilela Costa, Nucor Steel Brandenburg, Brandenburg, KY; and **Kip O. Findley** and **Robert L. Cryderman**, Advanced Steel Processing and Products Research Center (ASPPRC), Colorado School of Mines, Golden, CO. Contact e-mail: larissa.costa@nucor.com.

triding is unclear, particularly because the alloy is not designed to protect boron from boron nitride formation; that is, boron may not be in solution to promote hardenability. Additionally, there may be opportunity to promote grain refinement in alloys heat treated by low pressure carbonitriding by using Nb additions, similar to carburizing.

This work evaluates the fatigue performance of four different alloys, 20MnCr5, 20MnCr5 + B, SAE 8620, and SAE 8620 + Nb, after low pressure carbonitriding and pressurized gas quenching. Low pressure carbonitriding and gas quenching were designed to achieve a comparable hardness profile and effective case depth across all the alloys. Important parameters related to fatigue performance in low pressure carbonitriding and pressurized gas quenching are also analyzed such as hardness, retained austenite, residual stress, carbon and nitrogen profiles, prior austenite grain size, effective case depth, and microstructure in the surface and in the core of each specimen. Also, the influence of boron is evaluated by comparing 20MnCr5 with and without B additions. Additionally, the influence of Nb, added to control prior austenite grain size, is evaluated in the SAE 8620 alloys. While there are many similarities to carburizing, there is a low amount of literature on carbonitriding, especially low pressure carbonitriding treatments.

2. Methodologies

Low pressure carbonitriding and gas quenching were performed on Brugger specimens (Fig. 1) of the steel alloys 20MnCr5, 20MnCr5 + B, SAE 8620, and SAE 8620 + Nb. The Brugger specimens were machined from the hot-rolled cylindrical bars, and the fillet of each Brugger specimens was located at half radius of the total diameter of the cylinder, perpendicular to the rolling direction. The chemical composition of each steel alloy is shown in Table 1.

Low pressure carbonitriding and gas quenching (through pressurized nitrogen) were conducted at ECM-USA with the ICBP® Nano furnace that is well suited for heat treating small loads, such as the one used in this work. Thirty specimens of each of the four alloys were heat treated in the furnace in different batches. The carbonitriding pressure was 10.5 mbar, and the temperature was 920 °C, a temperature significantly higher than conventional carbonitriding treatments. Injections of acetylene, ammonia, and nitrogen were alternated during the heat treatment. Injections of ammonia were performed as the

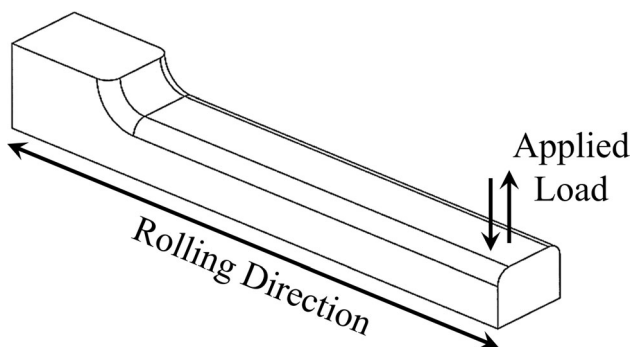


Fig. 1 Schematic showing Brugger specimen geometry and direction of the applied loads used for the fatigue tests

last steps in low pressure carbonitriding. Acetylene and ammonia were used to add carbon and nitrogen, respectively, and gaseous nitrogen was used to allow the diffusion of carbon and nitrogen through the steel. During the carbonitriding process, the addition of nitrogen between the injections of acetylene and ammonia are especially important also because acetylene (or other carburizing gas) and ammonia should not be mixed, as they can cause chemical reactions that are likely to produce more carbon due to the decomposition of other products (Ref 6). The specimens were quenched with pressurized nitrogen with different quenching pressures for the 20MnCr5 alloys and SAE 8620 alloys, due to the hardenability variation between them. The quenching pressure used for the 20MnCr5 and 20MnCr5 + B alloys was 4 bar, and for the SAE 8620 and SAE 8620 + Nb was 13 bar. The target surface hardness was 727 to 905 HV, the target core hardness was between 285 and 448 HV, and the target effective case depth (550 HV) was 0.65 to 0.75 mm. The specimens were tempered at 180 °C for two hours, with a total cycle of three hours including heating and cooling time. The parameters for carbonitriding are shown in Table 2.

Vickers hardness profiles, retained austenite profiles, residual stress profiles, carbon and nitrogen profiles, and average fatigue strength were obtained for all four alloys. For the hardness profiles, a LECO AMH55 Automated Hardness Indenter was used. Two different profiles were performed, with the one profile in the depth range between 100 and 1500 μm . The load for each indentation was 1 kgf, which was applied for 10 s. For the other profile, with a depth range near the surface between 20 and 120 μm , the load used was 25 gf.

Bending fatigue was performed on the low pressure carbonitrided Brugger specimens by using a SATEC Systems model SF-01U machine. The frequency of the tests was 30 Hz, and the R-ratio (minimum to maximum stress ratio) was 0.1. For these tests the “staircase method,” developed by Dixon and Mood (Ref 8), was employed to estimate the fatigue strength in each of the conditions.

X-ray diffraction was used to obtain the retained austenite volume fraction and the residual stress of each condition. For the retained austenite profile, a Siemens Kristalloflex 810, with a copper source ($\lambda = 1.5418 \text{ \AA}$) was used. The applied voltage and current were 30 kV and 25 mA, respectively. All the samples were analyzed with a 2θ range between 35° and 105° , step size of 0.05° , and step time 5 s. The residual stress analyses were conducted at the Stellantis facility in Auburn Hills, Michigan. The residual stress measurements were obtained by a Proto LXR (Proto Manufacturing Lab X-Ray Diffractometer Residual Stress Analysis System) using a chromium source operating at 30 kV and 25 mA and a spot size of 1 mm. The layers of each specimen were removed by electropolishing in a Proto Electropol.

Micrographs and fractographs were obtained with a JEOL JSM-7000F Field Emission Scanning Electron Microscope. The metallographic samples were cross sectioned from Brugger specimens, mounted in Bakelite, ground with 240, 320, 400, 600, and 1200 grit paper, polished with 6, 3, and 1 μm diamond paste, and etched with 2 pct nital. For fractography, the fractured specimens were rinsed with isopropyl alcohol before the analyses.

The average prior austenite grain size was measured on the surface (0 to 100 μm), in the effective case depth (650 to 750 μm), and in the core (> 1200 μm). Small samples were cut

Table 1 Chemical composition (wt.%) of the steel alloys 20MnCr5, 20MnCr5 + B, SAE 8620, and SAE 8620 + Nb

Alloy	C	Mn	Si	Ni	Cr	Mo	Ti	Nb	V	Al	B	N	S	P	Cu
20MnCr5	0.19	1.26	0.22	0.09	1.09	0.04	0.0005	0.002	0.003	0.023	0.0007	0.010	0.019	0.008	0.18
20MnCr5 + B	0.17	1.15	0.24	0.22	1.18	0.06	0.0046	0.003	0.026	0.033	0.0030	0.010	0.025	0.015	0.22
8620	0.21	0.87	0.14	0.47	0.56	0.20	...	0.002	...	0.017	0.0004	0.011	0.018	0.008	0.20
8620 + Nb	0.20	0.83	0.20	0.42	0.50	0.22	...	0.033	...	0.012	0.0003	0.006	0.020	0.009	0.17

Table 2 Recipe for low pressure carbonitriding treatments performed in the nano furnace at 920 °C

Gases injected into the furnace (NI/h)	Time of injection (s)
C ₂ H ₂	300
N ₂	500
NH ₃	300

from the Bruggen specimens, tempered at 300 °C for 20 hours and air cooled. Samples were mounted in Bakelite and ground with 320, 400, 600, and 1200 grit paper and polished with 6 and 3 micron diamond paste. After this process, the mounted samples were etched with a picral etchant consisting of 200 mL DI water, 2.6 grams of picric acid, 6 mL of Teepol, and 2 mL of HCl. The etchant was heated to approximately 70 °C and mixed until the picric acid was fully dissolved. A slight variation in the color of the reagent (from bright yellow to darker yellow) indicates that the reagent is ready to be used. The samples were immersed in the etchant for 30 seconds to 2 minutes and rinsed in ethanol. Back polishing was conducted to remove excessive etching. Microhardness indentations at depths of 100, 650, 750, and 1200 μm were used for reference for the location of the prior austenite grain size measurements. Approximately, 1000 grains were measured for each depth region in each alloy. For the measurements, several horizontal lines were traced on the micrographs by using ImageJ, and the number of intercepts were counted along the line to obtain the average and standard deviation of the prior austenite grain size for each alloy.

Carbon and nitrogen profiles were obtained through Glow-Discharge Optical Emission Spectroscopy (GDOES) at Spectra Analytik GMBH in Hof, Germany. The carbon and nitrogen profiles were obtained using a spot size (anode) of 2.5 mm. Measurements were performed according to ISO14707, ISO25138:2010, and ISO/DIS16962.2 (ISO/TC 201/SC 8). For this analysis, one Bruggen specimen of each alloy was tested with a depth range between 0 and 150 μm, and three analyses were obtained from each Bruggen specimen. The analyses were performed on the top and on the bottom of the Bruggen specimens.

Scanning transmission electron micrographs (STEM) were conducted on the FEI Talos F200X for the 20MnCr5 + B steel with the objective of identifying possible boron-based precipitates and other possible precipitates present in the alloy. The lift-outs were obtained in situ using the Helios NanoLab 600i DualBeam FIB/SEM.

Nano-SIMS was performed using the CAMECA IMS 6f at Arizona State University (ASU) to trace boron in the

Table 3 Hardenability expressed by the ideal diameter for each alloy (in mm)

Alloys	ID (mm)	Alloys	ID (mm)
20MnCr5	64.2	SAE 8620	52.9
20MnCr5 + B	64.9	SAE 8620 + Nb	47.7

20MnCr5 + B steel alloy. The sample was mounted with EpoThin 2 resin from Buehler, ground with 240, 320, 400, 600, 800, and 1200 grit SiC paper and polished with 9, 6, 3, 1, and 0.5 micron diamond paste. The analyses were performed in the core of the sample and on the hardened case, at approximately 400 μm from the corner surface.

3. Results and Discussion

The Caterpillar 1E0038 equation was used to calculate the hardenability in the steel alloys 20MnCr5, 20MnCr5 + B, SAE 8620, and SAE 8620 + Nb. Boron and niobium were not considered in these calculations, because the amount of these elements in solution is unknown. Hardenability is highest in the 20MnCr5 + B alloy followed by 20MnCr5, SAE 8620, and SAE 8620 + Nb, as shown in Table 3.

Bending fatigue data of the carbonitrided 20MnCr5, 20MnCr5 + B, SAE 8620, and SAE 8620 + Nb alloys were obtained through the “staircase method”, and the average fatigue strength values and standard errors were calculated through the Yoshimoto and Dixon and Mood methods (Ref 8, 9); the results are shown in Fig. 2. The average fatigue strength was higher for the 20MnCr5 alloys than for the SAE 8620 alloys. The difference in fatigue strength between SAE 8620 + Nb and SAE 8620 alloys is more significant than the difference in fatigue strength between 20MnCr5 + B and 20MnCr5 alloys.

Fatigue fracture features in the low pressure carbonitrided steels are similar to the fatigue fracture features obtained after gas or low pressure carburizing and oil quenching. For several of the fractured specimens for all four alloys, fatigue cracks clearly nucleated intergranularly on prior austenite grain boundaries, as shown in Fig. 3. The crack nucleation region in the 20MnCr5 + B steel is indicated in the figure with white arrows. In gas carburized steels, fatigue cracks nucleate intergranularly partly because of the intergranular oxidation that forms on the grain boundaries at the surface (Ref 10). According to Hyde (Ref 10), another potential reason for intergranular fatigue crack nucleation is due to the segregation of phosphorus to the grain boundaries. Intergranular oxidation does not form in steels heat treated through low pressure carburizing; however, the crack nucleation mechanism is still

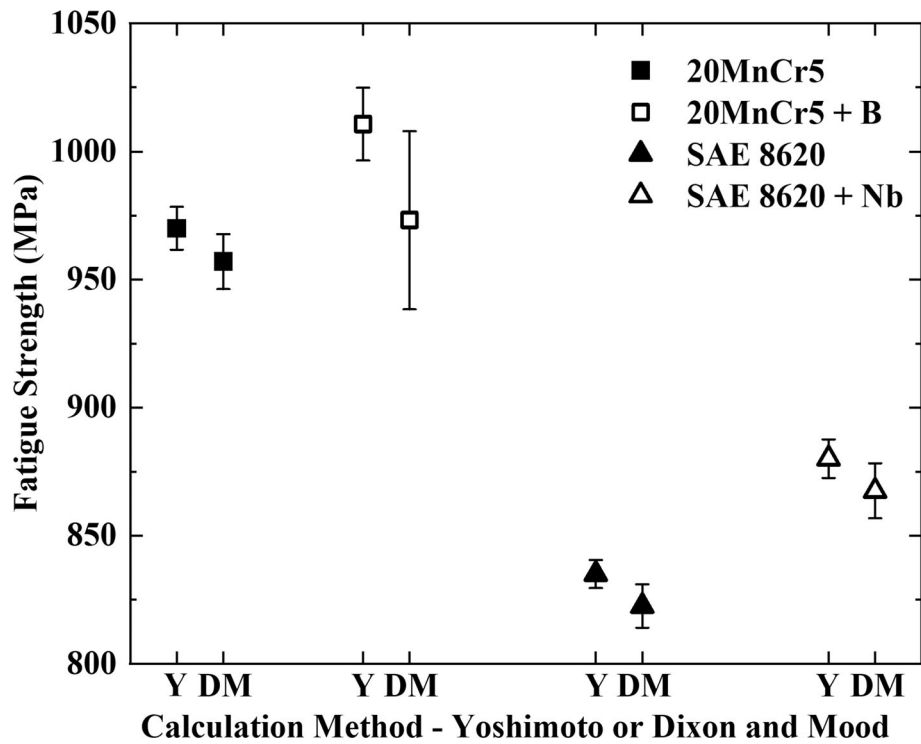


Fig. 2 Average and standard deviation of fatigue strength, calculated with the Yoshimoto, and Dixon and Mood methods for the 20MnCr5, 20MnCr5 + B, SAE 8620, and SAE 8620 + Nb alloys

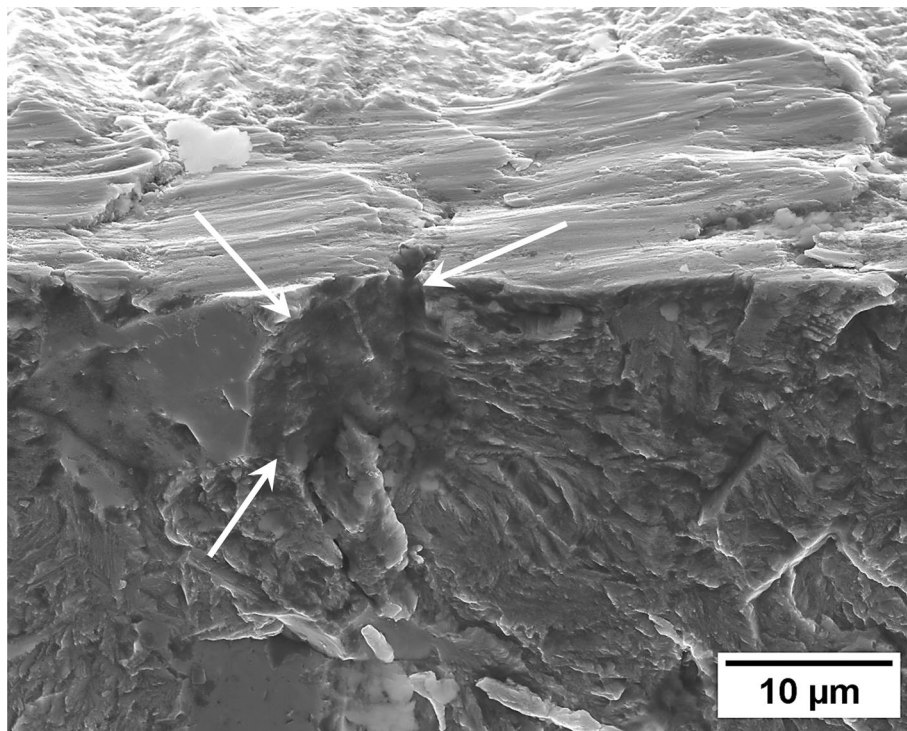


Fig. 3 Intergranular fatigue crack nucleation in a 20MnCr5 + B specimen showing that the crack nucleated on a prior austenite grain boundary. The failure occurred at maximum stress of 1000 MPa and 42,600 cycles

intergranular, often due to segregation of phosphorus to the grain boundaries. Similar to low pressure carburizing, low pressure carbonitriding does not form intergranular oxidation

either. Therefore, phosphorus segregation is one potential cause for intergranular fatigue crack nucleation in the low pressure carbonitrided steels. The phosphorus contents for 20MnCr5,

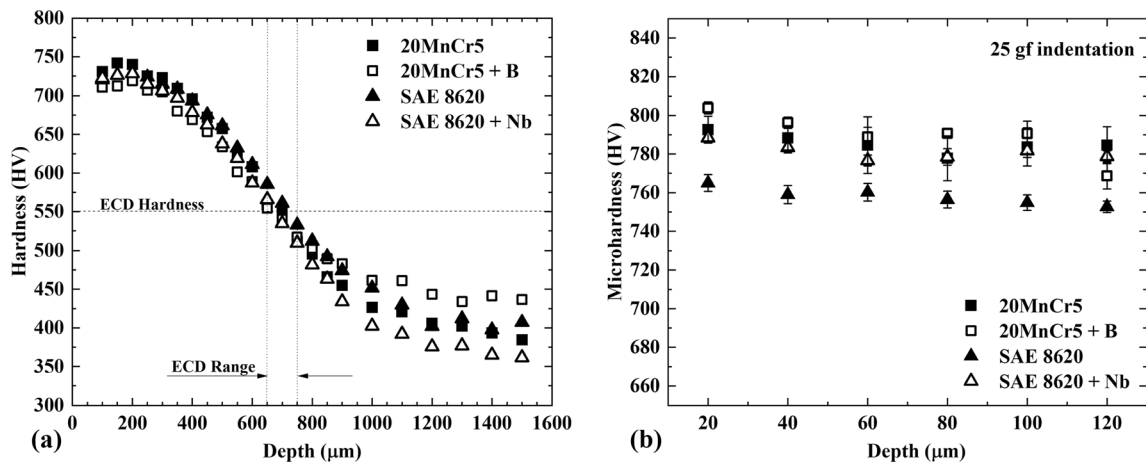


Fig. 4 Vickers hardness (a) average profile for all conditions and (b) average and standard error microhardness with 25 gf indentation in the range of 20–120 μm for all conditions

SAE 8620, and SAE 8620 + Nb are between 0.008 and 0.009 wt.%, and the phosphorus content in 20MnCr5 + B is slightly higher at 0.015 wt.%.

Hardness profiles for all the specimens were obtained after low pressure carbonitriding and pressurized gas quenching, as shown in Fig. 4a and b. The hardness profiles for all the specimens are very similar to each other from a depth of 100 μm to a depth of approximately 800 μm . After 800 μm , closer to the core, the hardness diverges, likely due to differences in hardenability. Due to the differences in composition of each alloy, the hardenability is higher in 20MnCr5 + B, followed by 20MnCr5, SAE 8620, and SAE 8620 + Nb. The 20MnCr5 + B alloy has the highest hardness in the core, and SAE 8620 + Nb has the lowest hardness, which corresponds to the lowest hardenability. In Fig. 4b, the average and standard error of hardness in the range of 20–120 μm are presented because this region is associated with fatigue crack nucleation and growth in the Bruggen fatigue specimens. The hardness values of 20MnCr5 + B, 20MnCr5, and SAE 8620 + Nb are statistically similar in this range, though 20MnCr5 + B has a higher hardness among these conditions, especially at depths closer to the surface, followed by 20MnCr5 and SAE 8620 + Nb. The SAE 8620 alloy has the lowest hardness among all alloys and is not statistically comparable to the other alloys.

The average and standard error of the prior austenite grain size are presented in Fig. 5 for each of the conditions evaluated. The base alloys SAE 8620 and 20MnCr5 have larger average prior austenite grain sizes compared to the modified alloys. The Nb additions in the SAE 8620 + Nb alloy were intended to promote niobium carbonitride precipitation during the heat treatment, and refine the average grain size. This microalloying concept has been employed for PAGS refinement in previous high temperature carburizing studies (Ref 11–13). The prior austenite grain size in the 20MnCr5 + B alloy is close to the prior austenite grain size of the SAE 8620 + Nb alloy, especially in the effective case depth and in the core regions, suggesting that the levels of aluminum, vanadium, boron, and titanium in this alloy compared to the other alloys promote grain refinement through nitride or carbonitride precipitates.

Average carbon and nitrogen profiles were obtained using GDOES for all the carbonitrided alloys, as shown in Fig. 6 and

7, respectively. Each point in both graphs represents data collected in a range of 1 μm from all three measurements. There is significant noise and uncertainty in the data in the first 2 μm ; therefore, this initial data was removed from the measurements. The amount of carbon in SAE 8620, in the range of 2–8 μm , is slightly higher than carbon content for the other alloys. Overall, the carbon contents near the surface and overall carbon profiles are similar for all of the alloys.

The initial target for nitrogen content was 0.2 wt.% for all the alloys; the nitrogen profile is near 0.2 wt.% at the surface, and it stabilizes in each alloy at values between 0.11 and 0.15 wt.%. Overall, the N content in the range measured by GDOES is more constant than carbon. For the 20MnCr5 + B condition, the nitrogen content was slightly higher than for the other alloys through the whole range analyzed. Both the 20MnCr5 and 20MnCr5 + B alloys had higher nitrogen contents on the surface compared to the 8620 alloys. One possibility for this higher nitrogen content could be due to the presence of elements with high affinity for nitrogen, especially boron, vanadium, and titanium. For the SAE 8620, the nitrogen content is slightly lower than for SAE 8620 + Nb. SAE 8620 + Nb also has niobium, which has a high affinity for nitrogen. Overall, it is possible that a significant part of the nitrogen content in this range analyzed through GDOES is in form of nitrides.

The retained austenite volume fraction profiles, at a depth between 0 and 100 μm , are shown in Fig. 8 for the 20MnCr5, 20MnCr5 + B, SAE 8620, and SAE 8620 + Nb alloys. Two or three measurements were made per alloy per depth, and all the retained austenite measurements are plotted on the graph for comparison. The retained austenite volume fraction on the surface of the steel alloys is lower than at deeper layers. One possible explanation is there is less constraint for the volume expansion associated with the martensitic transformation on the free surface of the alloys, thus promoting more transformation. According to Bepari (Ref 14), niobium as a microalloying element in carburized steels could lower the retained austenite volume fraction. In Fig. 8, there might be a slightly smaller amount of retained austenite in SAE 8620 + Nb compared to the other alloys, but the differences appear to be within the expected uncertainty of XRD measurements, as discussed in the ASTM E975-13 standard 0.

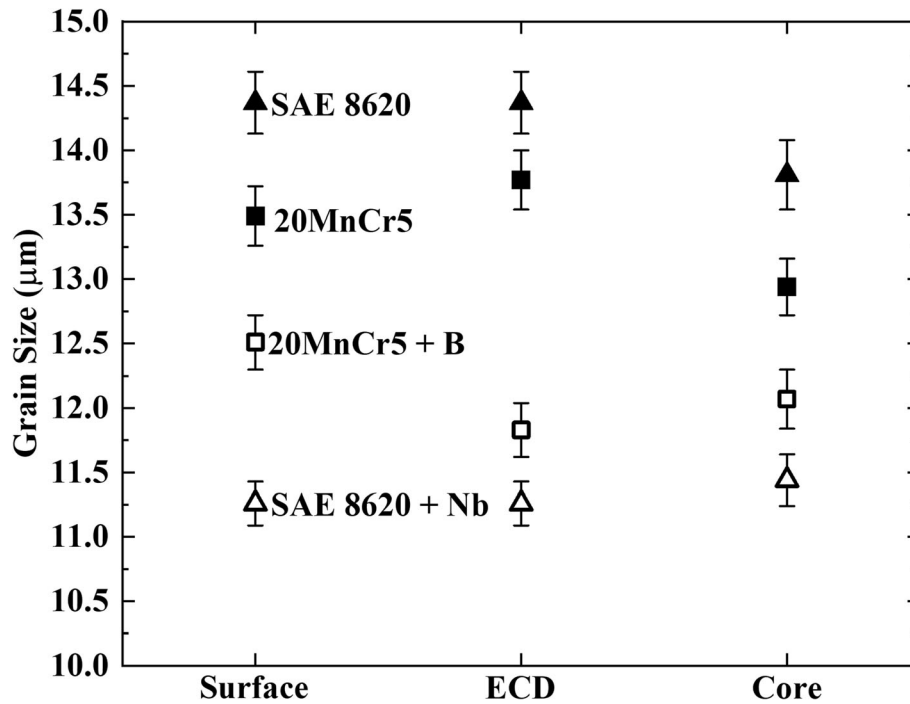


Fig. 5 Average and standard error values for prior austenite grain size of the steels after carbonitriding

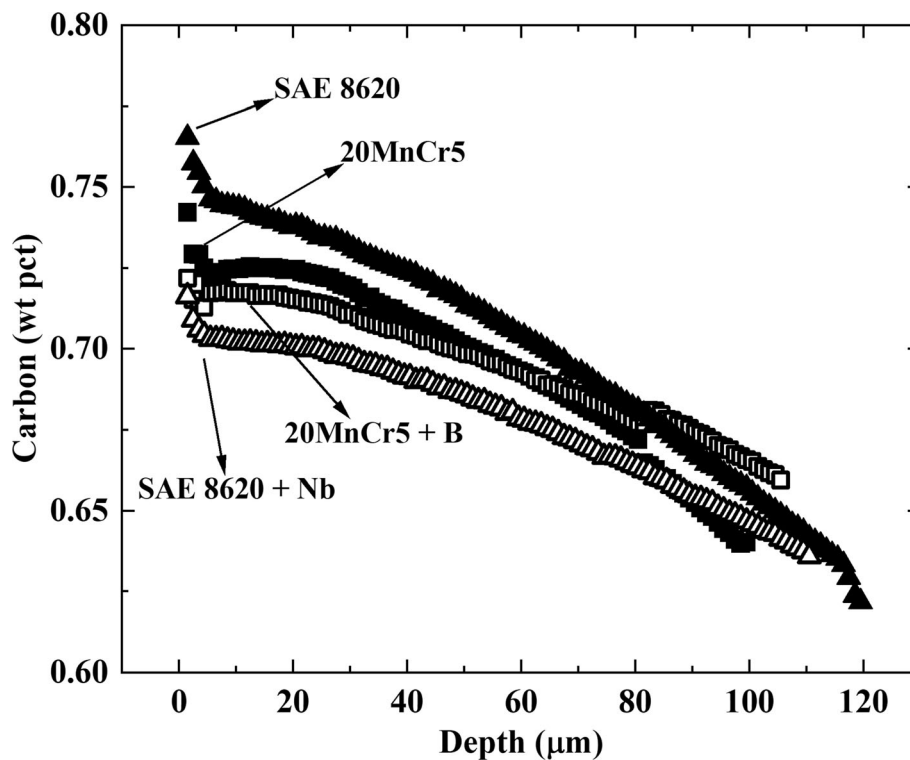


Fig. 6 Carbon profiles for all conditions after carbonitriding

The retained austenite volume fraction was also measured after fatigue on the surface of the 20MnCr5, 20MnCr5 + B, SAE 8620, and SAE 8620 + Nb alloys. For 20MnCr5 and 20MnCr5 + B, the fatigue specimens were run outs (the specimen reached 10^7 cycles without a failure) with a maximum applied stress of 950 and 1025 MPa, respectively.

The endurance limits, according to the Dixon and Mood calculation for these alloys, are 957 and 973 MPa, respectively. For the SAE 8620 and SAE 8620 + Nb, the fatigue specimens failed at 87,300 cycles at 875 MPa and 63,400 cycles at 900 MPa, respectively. The endurance limit for these alloys is 822 and 867 MPa, respectively. The retained austenite volume

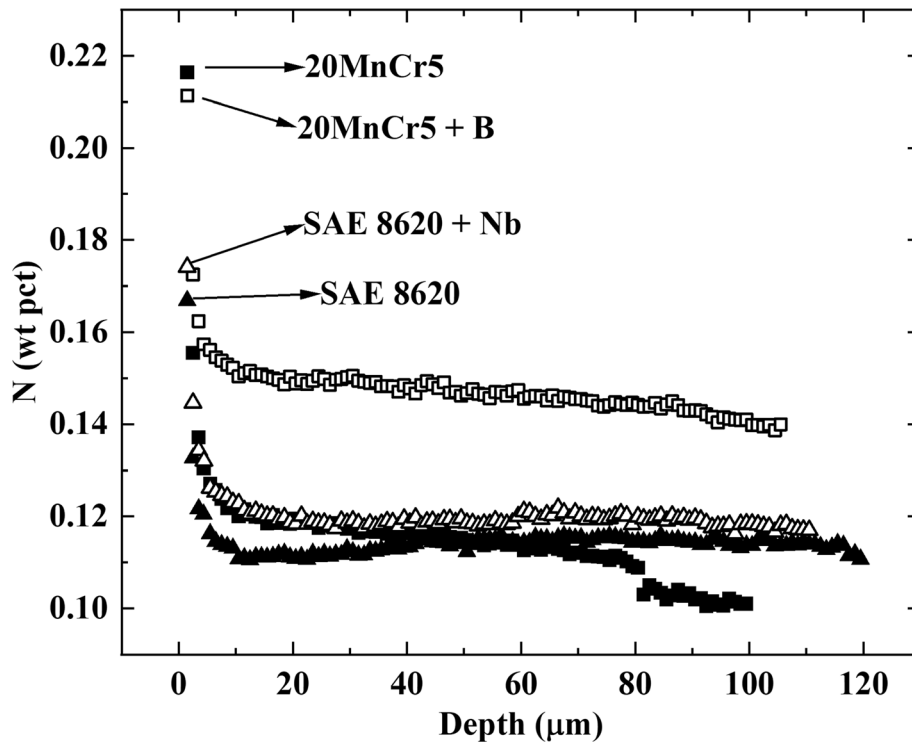


Fig. 7 Nitrogen profile for all conditions after carbonitriding

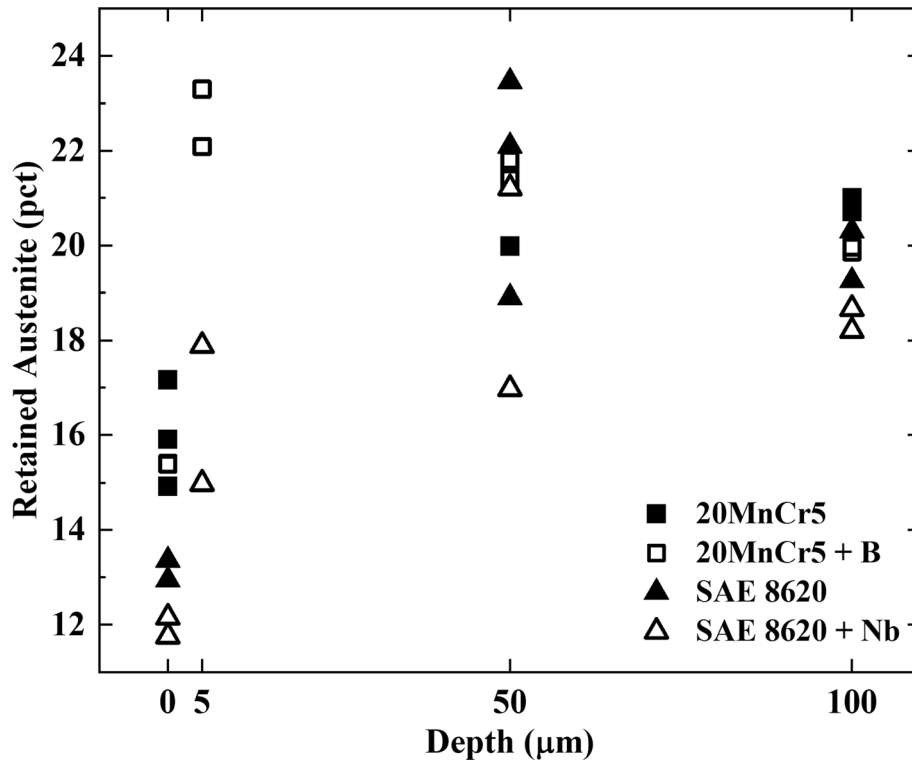


Fig. 8 Retained austenite volume fraction profile in 20MnCr5, 20MnCr5 + B, SAE 8620, and SAE 8620 + Nb, from the surface to 100 μm depth

fraction after the fatigue tests did not show a considerable variation, for either maximum applied stress close to the endurance limit (run out) or above the endurance limit (failure).

Surface residual stress is critical for fatigue performance. A high compressive residual stress on the surface alloys allows a higher maximum applied stress, since the effective stress on the specimen is the sum of the applied external stress and the

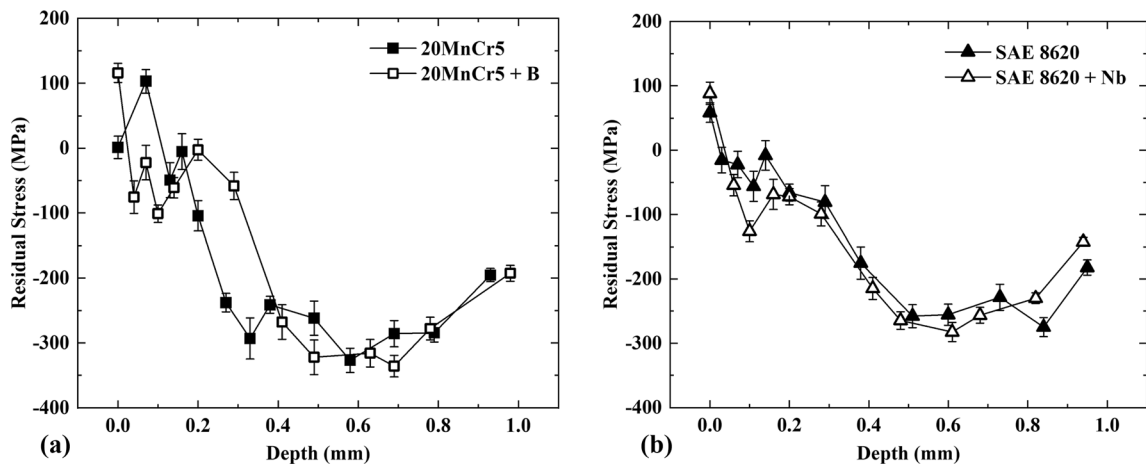


Fig. 9 Residual stress profiles obtained through XRD for the alloys (a) 20MnCr5 and 20MnCr5 + B and (b) SAE 8620 and SAE 8620 + Nb from the surface to 1 mm

residual stress (Ref 16). The residual stress profiles obtained through XRD, normal to the fracture plane, for all the alloys are shown in Fig. 9a and b, for the 20MnCr5 alloys and SAE 8620 alloys, respectively. The surface residual stress for all alloys is slightly tensile, becoming compressive at deeper layers. The residual stress profile is comparable for all the alloys, and even though there is a compressive residual stress near the surface, its magnitude is low compared to other surface hardening methods, including previous carburizing studies (Ref 10, 17).

Overall, the microstructure on the surface of all the alloys after low pressure carbonitriding and pressurized nitrogen quenching is a mixture of plate and lath martensite, and retained austenite. Some NMTPs, mostly Widmanstätten ferrite, in a martensitic matrix were found to various extents in all the alloys, as shown in Fig. 10a and b. The frequency that NMTPs appeared was different among each alloy, and they were significantly less frequent in the 20MnCr5 + B than in the other conditions. The presence of NMTPs on the surface of the alloys likely contributed to the tensile residual stress on the surface of the Bruggen specimens.

The presence of niobium-based precipitates in the SAE 8620 + Nb after carbonitriding, possibly niobium carbonitrides, were observed through micrographs and energy-dispersive X-ray spectroscopy (EDS), as shown in Fig. 11. The micrographs and EDS spectrum for the SAE 8620 + Nb were obtained at a depth of 25 μm from the surface. Lighter elements, such as nitrogen and carbon, cannot be accurately detected by this technique; therefore, it is not possible to detect what other elements besides niobium are also present in this particle. Although this particle is too large to be effective at pinning the grain boundaries, the refined average grain size in the SAE 8620 + Nb, indicates that finer particles are present also.

STEM images were obtained from lift outs on the surface of the 20MnCr5 + B, as shown in Fig. 12a and b. From Fig. 12a, energy-dispersive X-ray spectroscopy was performed on these samples, and the results indicate the precipitates are vanadium

and aluminum nitrides. From Fig. 12b, titanium nitrides were also found. Boron nitrides or $\text{M}_{23}(\text{B,C})_6$ precipitates were not found in these lift outs, but their presence is likely as boron is not fully protected from boron nitride formation at the heat treatment temperature. Vanadium nitrides and titanium nitrides possibly contribute to refined grain size in the 20MnCr5 + B alloy compared with the 20MnCr5 alloy.

According to Seah (Ref 18), carbon, boron, and nitrogen contribute the most to grain boundary cohesion of iron. They also have a propensity to segregate to grain boundaries because of their size, since they are interstitial atoms. The higher boron content in 20MnCr5 + B is one of the main differences between the alloys, and it is unknown if boron segregates to the grain boundaries of carbonitrided steel alloys, in the hardened case range.

Boron is one of the most difficult elements to trace, and nano-SIMS is one of the few techniques possible for this purpose. Nano-SIMS analysis was performed in two distinct regions of a 20MnCr5 + B sample, obtained from the cross-section of a Bruggen specimen. The core, where carbon and nitrogen contents are low, and the hardened case, where carbon and nitrogen contents are higher, were analyzed by this technique. The variation in colors indicate the intensity of each element in the map. Dark purple/blue colors indicate that the analyzed element is not present. As the colors change to brighter colors such as blue, light purple, red, orange, yellow, and white, the intensity of the element is higher.

A map in a region of the center of the sample was obtained with total exposure of approximately 11 hours. The area of this analysis is 20 μm \times 20 μm . Maps for boron and nitrogen were obtained, as shown in Fig. 13a and b, respectively. Nitrogen is not an easy element to trace since it does not get ionized like the other elements. Therefore, it is possible to have some interference from carbon in the nitrogen map. It is possible to observe that nitrogen is not uniformly distributed like carbon, and there are some regions of possible nitrogen segregation.

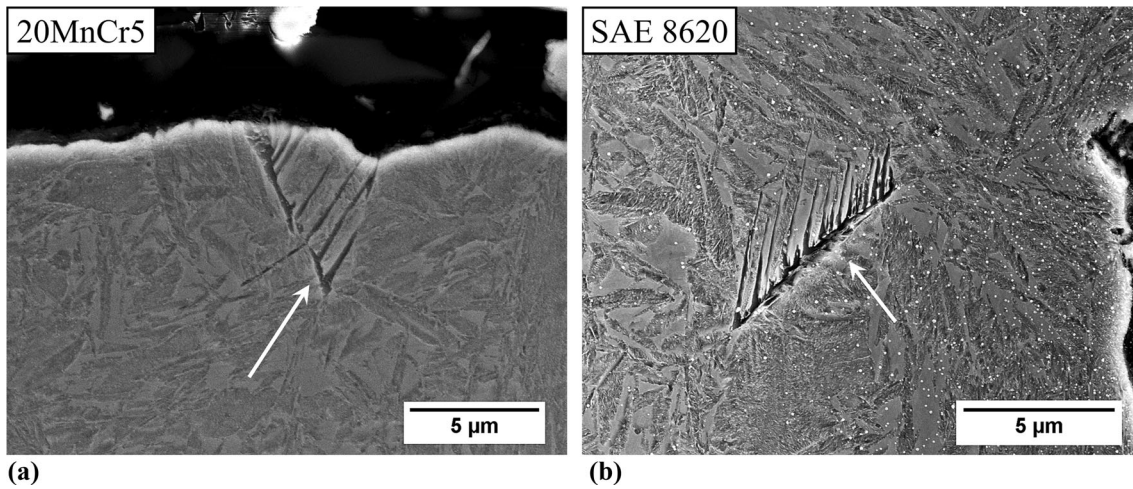


Fig. 10 Secondary electron micrographs showing the presence of NMTPs and a martensitic matrix in (a) 20MnCr5, (b) SAE 8620

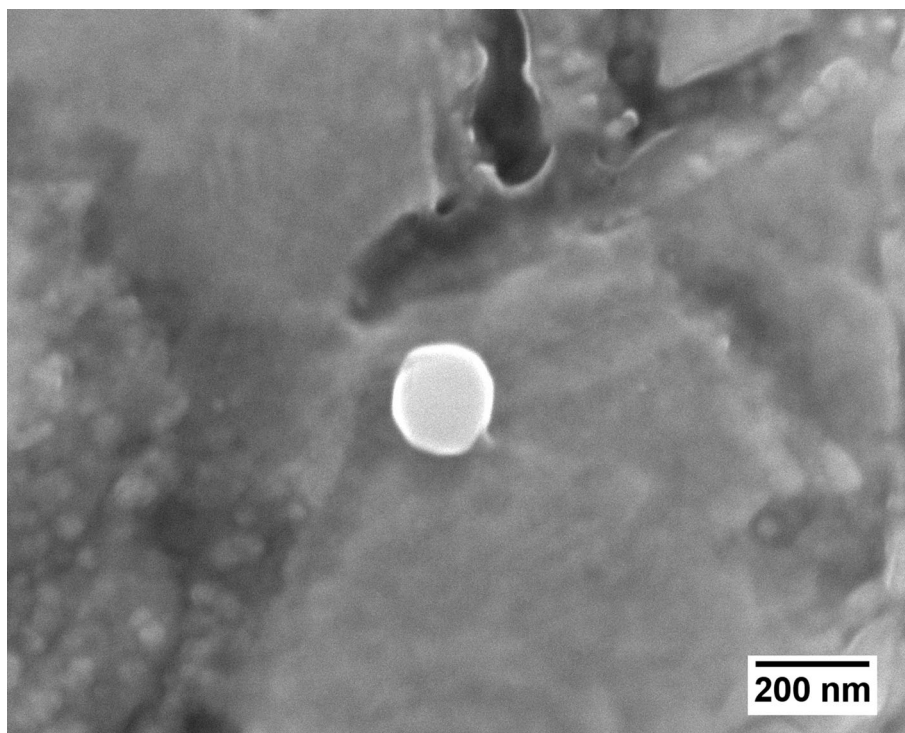


Fig. 11 Niobium-based secondary phase in the SAE 8620 + Nb alloy after carbonitriding, at 25 μm from the surface

An analysis on the edge of the specimen, at approximately 380 μm from the surface, was made in the hardened case region, as shown in Fig. 14. This analysis was performed for 4 hours, and a map of 50 $\mu\text{m} \times 50 \mu\text{m}$ for boron was obtained. Boron segregation such as the one detected in the core, did not occur in the edge. Boron seems to be more uniformly distributed in the case. The carbon and nitrogen content in this region is higher than that of the center of the specimen, and apparently the carbonitriding heat treatment changes the boron distribution, though there is still some boron segregation apparent. The boron segregation could be present on prior austenite grain boundaries, although this was not confirmed.

4. Conclusions

The effective case depth and surface hardness were comparable for all the alloys after low pressure carbonitriding and gas quenching. The carbon profile, nitrogen profile, retained austenite profile, residual stress profile, hardness profile, and retained austenite stability after fatigue were also comparable for the four heat treated alloys. Therefore, other characteristics were important for the fatigue performance of these alloys, such as the chemical composition and the average grain size of each alloy. Endurance limit was higher for the 20MnCr5 + B, followed by 20MnCr5, SAE 8620 + Nb, and SAE 8620.

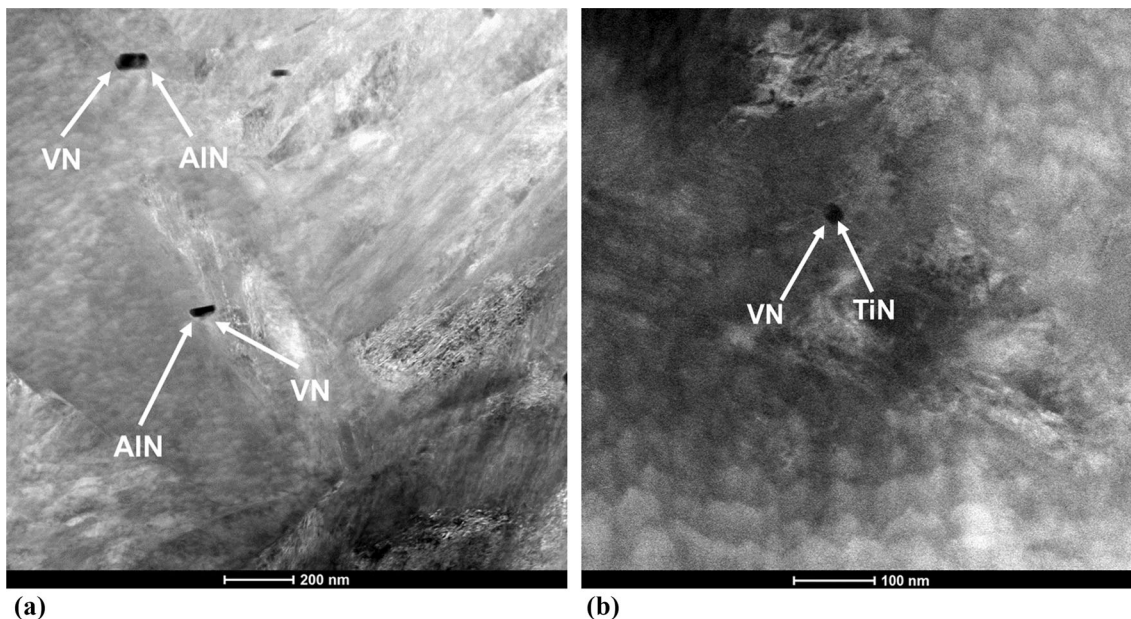


Fig. 12 STEM images obtained from a lift out of the 20MnCr5 + B surface showing (a) AlN and VN precipitates, and (b) VN and TiN precipitates

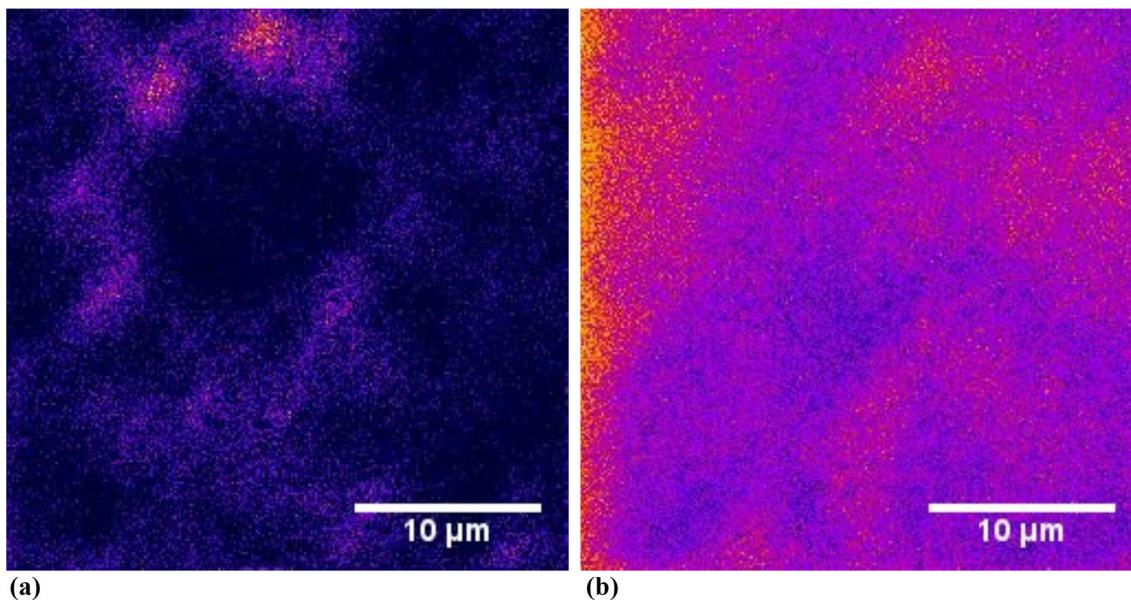


Fig. 13 Nano-SIMS maps in the central region of the 20MnCr5 + B sample of (a) boron, (b) nitrogen, after 11 hours of exposition

Boron segregation occurred in the core, and it is possible that this segregation occurred on the grain boundaries, as expected in a low carbon, low nitrogen steel, as observed through nano-SIMS. Although it is not completely clear that boron segregation occurs to the grain boundaries in the hardened case region. Overall, the mechanism of bending fatigue crack nucleation in low pressure carbonitrided specimens is intergranular in nature, which is similar to carburized heat treated specimens.

Boron behaved differently in environments with lower carbon and nitrogen contents (core), than those environments with high carbon and nitrogen contents (case). Boron segregated to the grain boundaries in the core of the steel alloys. Boron exhibited some segregation in the case, but its distribution was more uniform, suggesting that the carbonitriding process influences the boron distribution.

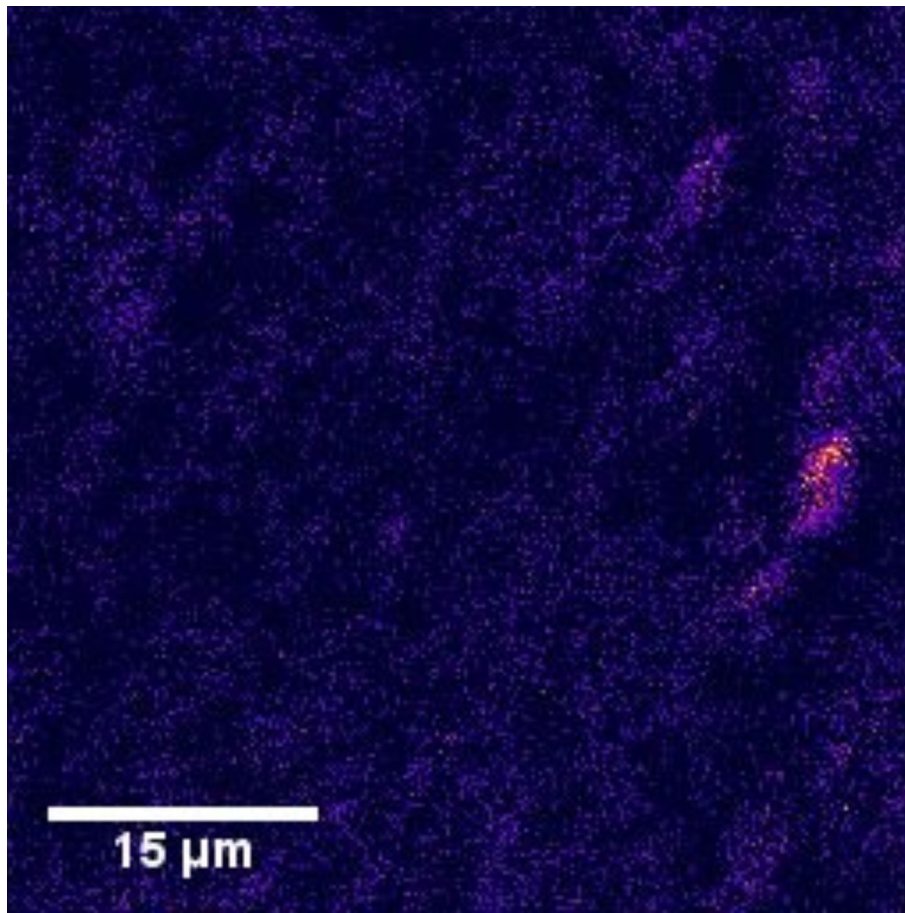


Fig. 14 Nano-SIMS maps on the edge of the 20MnCr5 + B sample for boron after 4 hours of exposure

The presence of NMTPs on the surface of all the alloys resulted in a tensile residual stress on the surface of the specimens.

Acknowledgments

The authors gratefully acknowledge the support of the Brazilian CNPq – Science without Borders program, the sponsors of the Advanced Steel Processing and Products Research Center (ASPPRC), especially Gerdau, CBMM North America, and FIAT-Chrysler North America, and the support of ECM-USA.

References

1. A. C. Ugural, *Mechanical Design of Machine Components*, 2nd edition, CRC Press, 2015
2. G.P. Cavallaro, T.P. Wilks, C. Subramanian, K.N. Strafford, P. French, and J.E. Allison, Bending Fatigue and Contact Fatigue Characteristics of Carburized Gears, *Surf. Coat. Technol.*, 1995, **71**, p 182–192
3. T. Marray, P. Jacquet, M. Mansori, A. Fabre, and L. Barrallier, A Thermodynamic and Experimental Study of Low Alloy Steels After Carbonitriding in a Low-Pressure Atmosphere, *Met. Sci. Heat Treat.*, 2014, **56**, p 434–439
4. C. Kanchanomai and W. Limtrakarn, Effect of Residual Stress on Fatigue Failure of Carbonitrided Low-Carbon Steel, *J. Mater. Eng. Perform.*, 2008, **17**, p 879–887
5. “Introduction to Surface Hardening of Steels,” In: *ASM Handbook Volume 4A*, pp. 393–395, ASM International. Materials Park, OH, 2013
6. T. Hoffman M. Steinbacher, B. Clausen, S. Bischoff, H. Klümper-Westkamp, and H. Zoch, “New Carbonitriding Processes”, *Proceedings of 26th ASM Heat Treating Society Conference*, pp. 115–121, 2011
7. A. Goldsteinas, “New Vacuum Processes Achieve Mechanical Property Improvement in Gearbox Components” *Industrial Heating*, May 2007
8. D.J. Dixon and A.M. Mood, A Method for Obtaining and Analyzing Sensitivity Data, *J. Am. Stat. Assoc.*, 1948, **43**(241), p 109–126
9. I. Yoshimoto, Fatigue Test by Staircase Method with Small Samples, *Bulletin of JSME*, 1962, **15**(18), p 211–221
10. R.S. Hyde, “Quench Embrittlement and Intergranular Oxide Embrittlement: Effects on Bending Fatigue Initiation of Gas-Carburized Steel,” Ph.D. Thesis, Colorado School of Mines, Department of Metallurgical and Materials Engineering, 1994
11. R.E. Thompson, “Microstructural Development and Fatigue Behavior of Niobium Modified Carburizing Steels,” MS Thesis, Colorado School of Mines, Department of Metallurgical and Materials Engineering, 2007
12. D.K. Matlock, K.A. Alogab, M.D. Richards, and J.G. Speer, Surface Processing to Improve the Fatigue Resistance of Advanced Bar Steels for Automotive Applications, *Mater. Res.*, 2005, **8**, p 453–459
13. C.M. Enloe, K.O. Findley, J.G. Speer, A. Shibata, D. Terada, and N. Tsuji, “The Effects of Mo and Initial Precipitate Distribution on (Nb,Ti)(C,N) Precipitate Size Evolution in a High-Temperature Carburizing Steel,” *Proceedings of the 3rd International Symposium on Steel Science (ISSS-2012)*, ISIJ, Tokyo, pp. 163–166
14. M.M.A. Bepari and K.M. Shorowordi, Effects of molybdenum and nickel additions on the structure and properties of carburized and hardened low carbon steels, *J. Mater. Process. Technol.*, 2004, **155–156**, p 1972–1979

15. ASTM E975-13 standard ASTM Standard Practice, “Standard Practice for X-Ray Determination of Retained Austenite in Steel with Near random Crystallographic Orientation”, ASTM E975-13, 2013
16. “Failure Analysis and Prevention,” In: ASM Handbook Volume 11, Materials Park, OH: ASM International, 2013
17. J.A. Sanders, “The Effects of Shot Peening on the Bending Fatigue Behavior of a Carburized SAE 4320 Steel,” MS Thesis, Colorado School of Mines, Department of Metallurgical and Materials Engineering, 1993
18. M. Seah, Adsorption-Induced Interface Decohesion, *Acta Metall.*, 1980, **28**, p 955–962

Publisher's Note Springer Nature remains neutral with regard to jurisdictional claims in published maps and institutional affiliations.

Springer Nature or its licensor (e.g. a society or other partner) holds exclusive rights to this article under a publishing agreement with the author(s) or other rightsholder(s); author self-archiving of the accepted manuscript version of this article is solely governed by the terms of such publishing agreement and applicable law.